Quantum Electronics **51** (9) 812–818 (2021)

https://doi.org/10.1070/QEL17616

Polarisation gating technique in nonlinear Compton scattering: effect of radiation friction and electron beam nonideality

M.A. Valialshchikov, V.Yu. Kharin, S.G. Rykovanov

Abstract. **We discuss the effect of radiation friction and quantum recoil on the parameters of a gamma comb with narrow spectral peaks, arising when use is made of laser pulses with time-dependent polarisation, which reduces significantly the ponderomotive broadening of harmonics. A detailed numerical study of the contribution of the electron beam nonideality to the observability of the effect is presented.**

Keywords: *Compton scattering, Thomson scattering, polarisation gating technique, harmonic generation, gamma radiation, ponderomotive broadening.*

1. Introduction

Nonlinear Compton scattering is a promising method for obtaining X-ray and gamma radiation. Recent progress in the field of laser-plasma accelerators has increased interest in compact Compton photon sources [1–6]. Such sources have a number of useful properties: monochromaticity, tunability, high intensity, and low angular divergence. Due to this, they can be useful in medicine [7, 8], ultrafast radiography [9, 10], nuclear photonics [5], and other fields [11]. Since the cross section of the Compton scattering process is extremely small, it is natural to increase the laser pulse intensity in order to obtain a brighter source. However, for more intense laser pulses, their magnetic field begins to strongly affect the dynamics of electrons. The presence of an envelope in a laser pulse essentially modulates the electron motion, which causes a significant broadening of the emitted spectrum (spectral ponderomotive broadening) [12–16]. This effect greatly limits the applicability of Compton sources at large laser field amplitudes.

To avoid this broadening, various methods have been actively developed for a long time, for example, it has been proposed to use flat-top laser pulses [17] or a chirped laser pulse, the frequency of which varies nonlinearly to compensate for the envelope influence [18, 19]. These methods are rather difficult to implement experimentally for high laser intensities; however, it has recently been shown that it is sufficient to use only a linear chirp to significantly reduce ponderomotive broadening [20, 21]. It has also recently been proposed to use laser pulses with time-dependent polarisation (the so-called polarisation gating technique [22]) in order to avoid ponderomotive broadening of the harmonic spectrum [23]. This method is based on the fact that, at sufficiently high intensities, harmonics of the fundamental Compton line appear in the spectrum of backscattered radiation upon scattering a linearly polarised pulse, which is not the case of the scattering of a circularly polarised pulse. The polarisation gating technique makes it possible to limit the emission of harmonics to the time region near the laser intensity maximum, where the polarisation is close to linear, and the intensity gradient is smaller, which significantly reduces the ponderomotive broadening and leads to the presence of a gamma comb of spectrally narrow harmonics.

Note that at high laser intensities the spectra of adjacent harmonics begin to overlap, and the entire spectrum looks rather disorderly; however, when use is made of the polarisation gating technique, the harmonics form a narrow gamma comb. In work [23], the method itself is described in more detail, the results of numerical simulation from the viewpoint of classical electrodynamics are presented, and it is also shown that for the parameters of laser radiation of interest, the effect of radiation friction can be neglected, since it only leads to a small frequency red-shift.

This work is dedicated to a more detailed analysis of the polarisation gating technique, namely, the effect of the classical radiation friction and the quantum recoil on the gamma comb is considered, since the contribution of these effects increases with increasing laser intensity and harmonic's number. Moreover, by measuring the spectral shift of the harmonic peaks relative to their classical position, it is possible to experimentally estimate the quantum shift of high harmonics for relatively intense laser pulses with a normalised vector potential amplitude $a_0 \geqslant 1$ ($a_0 = eA_{las}/mc^2$, where A_{las} is the laser amplitude; and e and m are the absolute values of the electric charge and electron mass, respectively). A numerical study of the effect of the parameters of the electron and laser beams on the gamma comb observability was also performed. The paper uses the natural system of units $\hbar = c = 1$, and the spatial and energy units become dimensionless using the initial laser frequency ω_{las}: $x\,\omega_{las} \to x$, $\omega/\omega_{las} \to \omega$.

2. Methods

The polarisation gating technique consists in the generation of laser pulses with time-dependent polarisation. The experimental implementation of this method is not very complicated, for example, various nonlinear optical schemes can be used [22]. By adding laser pulses with right- and left-hand cir-

M. A. Valialshchikov, S. G. Rykovanov Skolkovo Institute of Science and Technology, Skolkovo Innovation Centre, Bolshoi bul'var 30, stroenie 1, 121205 Moscow, Russia; e-mail: serge.rykovanov@gmail.com; **V.Y. Kharin** Genity LLC, 444 W. Lake Street, Chicago, Illinois, USA, 60606

Received 5 July 2021
Kvantovaya Elektronika **51** (9) 812–818 (2021)
Translated by M.A. Monastyrskiy

cular polarisation with a certain delay of the pulses relative to each other, it is possible to obtain a laser pulse with circular polarisation at the front and rear edges and with linear polarisation at the centre. The vector potential of such a pulse, with the allowance for the envelope phase effects, is as expressed as:

$$A_\perp = \frac{a_0}{2} e^{i\varphi}\left[g\left(\varphi - \frac{\delta}{2}\right)e^{-i\delta/2}\epsilon_+ + g\left(\varphi + \frac{\delta}{2}\right)e^{i\delta/2}\epsilon_-\right] + \text{c.c.}, \quad (1)$$

where $g(\cdot)$ is the time envelope; $\varphi = t - z$ describes the laser pulse front; δ is the delay between two circularly polarised pulses; and $\epsilon_\pm = [1, \pm i]^T$ is the ellipticity parameter corresponding to right- or left-hand circular polarisation. Note that to ensure linear polarisation at $\varphi = 0$, the condition $\delta = \pi n$ must be satisfied, where n is an integer.

In the classical formalism, the radiation of an electron is completely determined by its trajectory. In our formulation of the problem, the laser pulse moves in the positive direction of the $+z$ axis, and the electron moves towards the pulse. Next, we will work in the coordinate system in which the electron is initially at rest, $p = (m, 0, 0, 0)$, and the quantities of interest can be obtained in the laboratory system using the Lorentz transformations.

If we do not take into consideration the radiation friction, the trajectories are obtained by integrating the equations of relativistic motion with the Lorentz force in the right-hand side. For a plane wave, there are symmetries with respect to translations in space and the light cone $(t - z)$, and an analytical solution for the 4-velocity u is known (in our case, the electron was initially at rest) [24]:

$$u^0 - u^3 = 1, \quad (2)$$

$$\boldsymbol{u}_\perp = \boldsymbol{A}_\perp, \quad (3)$$

$$u^0 + u^3 = 1 + A_\perp^2. \quad (4)$$

Taking into account the radiation friction force, it is necessary to solve the Lorentz–Abraham–Dirac (LAD) equation [25]. If the characteristic wavelength and the external field amplitude E satisfy the condition $\lambda \gg \alpha\lambda_C$, $E \ll E_{cr}$ [where $\alpha \approx 1/137$ is the fine structure constant; λ_C is the Compton wavelength; and E_{cr} is the critical electromagnetic field of quantum electrodynamics (QED)], the LAD equation transforms into the Landau–Lifshitz equation [25]:

$$\frac{du^\mu}{ds} = -F^{\mu\nu}u_\nu + \frac{2}{3}\frac{\alpha}{m} \times[(\partial_\alpha F^{\mu\nu})u^\alpha u_\nu - F^{\mu\nu}F_{\alpha\nu}u^\alpha + (F^{\alpha\nu}u_\nu)(F_{\alpha\lambda}u^\lambda)u^\mu], \quad (5)$$

where $F^{\mu\nu} = \partial^\mu A^\nu - \partial^\nu A^\mu$ is the electromagnetic tensor. This equation can be solved numerically [26, 27], and in the case of a plane wave, analytical expressions for the 4-velocity can be used [28].

The spectral radiation intensity per unit solid angle can be obtained using the formula [29]:

$$\frac{d^2I}{d\omega d\Omega} = \frac{\omega^2}{4\pi^2} \times\left|\int_{-\infty}^{\infty} d\varphi\, \boldsymbol{n}\times[\boldsymbol{n}\times\boldsymbol{u}]\exp[i\omega(\varphi + z - \boldsymbol{nr})]\right|^2, \quad (6)$$

where $d\Omega$ is the solid angle element, and $\boldsymbol{n}$ is the unit vector directed from the origin to the observation point. To obtain energy (in ergs), it is necessary to multiply the dimensionless values by $e^2\omega_{las}$.

From equation (6), we obtain the centre frequencies of harmonics on the axis in the reference frame in which the electron was initially at rest (without taking into account radiation friction):

$$\omega_n^{cl} = \frac{n}{1 + A_\perp^2}, \quad (7)$$

where $n = 2k + 1$ is a nonnegative integer denoting the harmonic number. In the laboratory system, the frequencies have an additional factor $4\gamma^2$.

There are several methods for numerical calculation of the integral in equation (6); for example, we can consider this integral as a Fourier transform in terms of retarded time and use the fast Fourier transform for efficient calculation [30].

From the point of view of quantum electrodynamics, Compton nonlinear scattering is described as a first-order process in the Furry picture using the well-known solutions of the Dirac equation in an external field – Volkov states [31]. For an electron with an initial 4-moment p^μ and spin polarisation σ, the positive-energy ($p_0 > 0$) Volkov state $\Psi_{p\sigma}$ has the form:

$$\Psi_{p\sigma}(x) = \left[1 - \frac{\hat{k}\hat{A}}{2(kp)}\right]u_{p\sigma}e^{iS_p}, \quad (8)$$

where k is the wave vector of the incident pulse; $\hat{v} = \gamma_\mu v^\mu$ for an arbitrary 4-vector v^μ; $u_{p\sigma}$ is a positive-energy free bispinor normalised to unity: $\bar{u}_{p\sigma}u_{p\sigma} = 1$ (the upper bar denotes the Dirac conjugation); and

$$S_p = -(px) - \int_{-\infty}^{\varphi} d\varphi'\left[-\frac{(pA(\varphi'))}{(kp)} - \frac{A^2(\varphi')}{2(kp)}\right] \quad (9)$$

is the classical action of electron in a plane wave.

Then, for the process of emission of a single photon by a single electron, the scattering amplitude takes the form

$$M_{\varepsilon\sigma'\sigma}^{qp} = -i\int \overline{\Psi}_{q\sigma'}(x)\hat{\varepsilon}^* e^{i(\kappa x)}\Psi_{p\sigma}(x)d^4x, \quad (10)$$

where ε is the polarisation vector of the emitted photon and $\kappa^\mu = (\omega, \boldsymbol{\kappa})$ is its wave 4-vector.

Recall that we are working in the reference frame in which the electron was initially at rest; therefore, the expressions for the Volkov states and the transition amplitude take a simpler form. In numerical calculations, to obtain the differential probability of photon emission per unit frequency and unit solid angle, we used the amplitudes of the transition probabilities between Volkov states, summing them over the polarisations of the emitted photon and electron and averaging them over the initial projection of the electron spin

$$\frac{dN_{ph}}{d\omega d\Omega} = \frac{\alpha}{16\pi^2}\frac{m\omega}{m - \omega + \kappa^3}\frac{1}{2}\sum_{\varepsilon\sigma\sigma'}|M_{\varepsilon\sigma'\sigma}|^2. \quad (11)$$

In this case, the centre frequencies of the harmonics on the axis are given by the expression:

$$\omega_n^{QED} = \frac{n}{1 + A_\perp^2 + n\chi}, \quad (12)$$

where $\chi = 2\omega_{las}/m$ is the photon recoil (in the laboratory system, χ has a multiplier of 2γ, and frequencies have a multiplier of $4\gamma^2$). It can be seen from formulae (7) and (12) that the spectral positions of harmonics on the beam axis for the clas-

sical and quantum cases differ by the recoil value, which is more significant for higher harmonics. Note that the distance between two peaks in the classical formalism is

$$\Delta\omega^{\mathrm{cl}} = \omega^{\mathrm{cl}}_{n+2} - \omega^{\mathrm{cl}}_{n} = \frac{2}{1 + A_{\perp}^{2}},$$

while the difference between the classical and quantum positions of the harmonics is

$$\Delta\omega^{\mathrm{cl-QED}} = \omega^{\mathrm{cl}}_{n} - \omega^{\mathrm{QED}}_{n} = \frac{n^2\chi}{(1 + A_{\perp}^{2})(1 + A_{\perp}^{2} + n\chi)}.$$

If $\Delta\omega^{\mathrm{cl-QED}}$ is not too small, the difference can be measured experimentally.

From now on, we will use a Gaussian envelope with a centre at φ_0 and a half-width τ: $g(\varphi) = \exp[-(\varphi - \varphi_0)^2/\tau^2]$. Also, only optimally polarisation gated pulses that form a gamma comb in the spectrum will be considered (for a Gaussian envelope, this means that the delay between the pulses is $\delta = \tau$, see work [23]). Numerical simulation for a single electron in the classical formalism was carried out using the Fourier transform method, while the VDSR code was used for the classical radiation friction force and scattering by an electron beam [32]. The electron beam parameters are typical for modern accelerator facilities, for example, for DESY FLASH [33].

3. Results

This section is arranged as follows: in Section 3.1, we consider the effect of the classical force of radiation friction and quantum recoil on the backscattered spectrum and angular distribution of radiation in the case of scattering by a single electron, and in Section 3.2 we analyse the effect of ponderomotive scattering and electron beam nonideality on the gamma comb observability, and also present calculations for scattering by an electron beam with regard to the classical force of radiation friction.

3.1. Scattering by a single electron

Figure 1 shows the vector potential and the ellipticity parameter for an optimally polarisation gated pulse ($a_0 = 2, \tau = 10\pi$) and the corresponding backscattered spectrum by a single electron ($\gamma = 1000$). Once again, we note that in such a pulse the polarisation is linear at the centre and circular at the wings. By limiting the emission of harmonics to the region around the laser pulse peak, where the intensity gradient is smaller and the harmonic radiation efficiency is higher, we obtain a gamma comb in the backscattered spectrum with each harmonic being narrow. Since the polarisation gating technique does not affect the ponderomotive broadening of the fundamental line, an interference pattern of the fundamental line and two harmonics falling into this interval can be observed in the region of $\omega/4\gamma^2 < 1$. If we considered the spectrum for an ordinary Gaussian pulse of similar intensity (the amplitude a_0 is specified for a single circularly polarised pulse, and so the effective intensity for a single Gaussian pulse will be higher), the harmonics would overlap, and the entire spectrum would be complex. The spectrum dependence on the delay between two pulses and the effect of the intensity and laser pulse duration on the distance between the peaks and the width of the peaks in the gamma comb are considered in work [23].

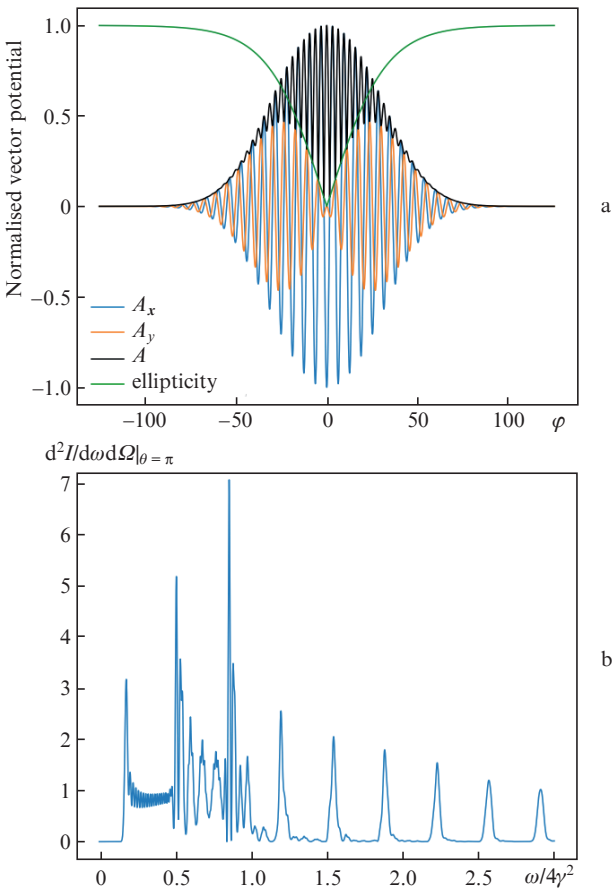

Figure 1. (Colour online) Normalised vector potential of an optimally polarisation gated pulse and its ellipticity; $A = (A_x, A_y, 0)$ is the 3-vector potential, laser pulse parameters: $a_0 = 2$, $\tau = 10\pi$; for an electron $\gamma = 1000$ (a), and (b) is the corresponding backscattered spectrum.

For high field intensity and electron energy, the effect of radiation friction becomes more and more noticeable. Therefore, it is of interest to see how the inclusion of the radiation friction force in the classical formalism or the recoil of electron in QED affects the gamma comb. Figure 2 shows the differential number of photons in the backscattered spectrum (in the reference frame where the electron was initially at rest) in the simulation without the radiation friction, in the simulation taking into account the radiation friction in the framework of the Landau–Lifshitz equation and in the simulation taking into account the electron recoil in the framework of the QED formalism for the cases $a_0 = 1$, $\tau = 16\pi$ and $a_0 = 1.4$, $\tau = 16\pi$. The main difference from the classical case is the red shift of harmonics, the value of which is consistent with formula (12), while the ponderomotive broadening caused by these effects is not so noticeable. For higher laser intensities, the situation changes, since the radiation friction leads to a significant broadening of the spectrum over the entire interval between adjacent peaks of the comb.

In addition, for higher harmonics and electron energies, the difference between classical and quantum predictions becomes more significant. For example, for the first case [$a_0 = 1, \tau = 16\pi, \gamma = 1000, \lambda_{\mathrm{las}} = 0.8$ μm (λ_{las} is the laser wavelength)] $\Delta\lambda_5^{\mathrm{cl-QED}}/\lambda_5^{\mathrm{cl}} \approx 2.7 \times 10^{-2}$, where $\Delta\lambda_5^{\mathrm{cl-QED}}$ is the difference between the classical and quantum predictions for the wavelength of the fifth harmonic, $\lambda_5^{\mathrm{cl}} \approx 8.9 \times 10^{-5}$ nm. At a lower electron energy ($\gamma = 10$), the difference becomes smaller:

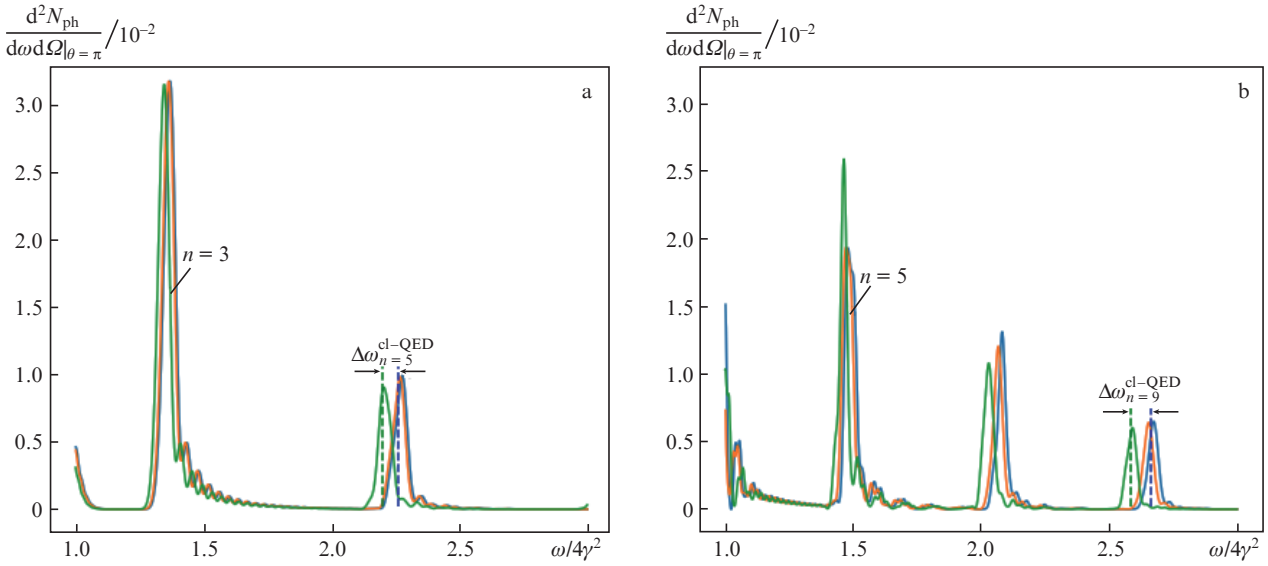

Figure 2. (Colour online) Differential number of photons in the spectrum of backscattering by a single electron (in the reference frame where the electron was initially at rest) of an optimally polarisation gated pulse simulated with allowance for the Lorentz force (blue curve), the classical radiation friction force in the framework of the Landau–Lifshitz equation (orange curve) and QED formalism (green curve) for (a) $a_0 = 1$, $\tau = 16\pi$, and (b) $a_0 = 1.4$, $\tau = 16\pi$. Blue dashed line shows the classical position of the harmonic corresponding to formula (7), and the green dashed line shows the quantum prediction of the harmonic position corresponding to formula (12).

$\Delta\lambda_5^{cl-QED}/\lambda_5^{cl} \approx 2.7 \times 10^{-4}$, $\lambda_5^{cl} \approx 8.9 \times 10^{-1}$ nm. In the second case ($a_0 = 1.4$, $\tau = 16\pi$, $\gamma = 1000$) for high harmonics, it can be seen that the difference between the predictions becomes even greater. In the QED formalism, the following estimates can be given for the probability of photon emission by an electron for the entire time of interaction with a laser pulse: in the first case $N_{ph} \approx 0.52$, and in the second $N_{ph} \approx 0.91$.

The broadening caused by radiation friction becomes more noticeable when considering the angular distribution. Figure 3 shows the angular distribution of the laser radiation scattering spectrum (at $a_0 = 1.4$ and $\tau = 16\pi$) for a plane with a polar angle equal to zero. For the classical case, the gamma comb is clearly visible in the entire region under consideration, and, taking into account the radiation friction, the greater the distance from the axis, the more blurred the spectrum. Therefore, it is most likely worth using smaller collimation angles.

3.2. Scattering by an electron beam

The results of numerical simulation of the scattering of a laser pulse by an electron beam are presented here. The laser pulse is considered in the paraxial approximation, with the beam size w_0 at the focus. An electron beam consisting of 10^8 electrons (16 pC) is represented by 2400 macroparticles and is characterised by a normalised emittance ($\epsilon_n = \sigma_r\sigma_p$, where σ_r is the radial divergence and σ_p is the momentum spread), a central gamma factor $\gamma = 1000$ and an energy divergence δE.

It is of interest to see how many photons can be obtained in a single peak of the gamma comb. According to equation (6), the differential number of photons is obtained from the relation

$$\frac{d^2N_{ph}}{d\omega d\Omega} = \alpha\frac{1}{\omega}\frac{d^2I}{d\omega d\Omega},$$

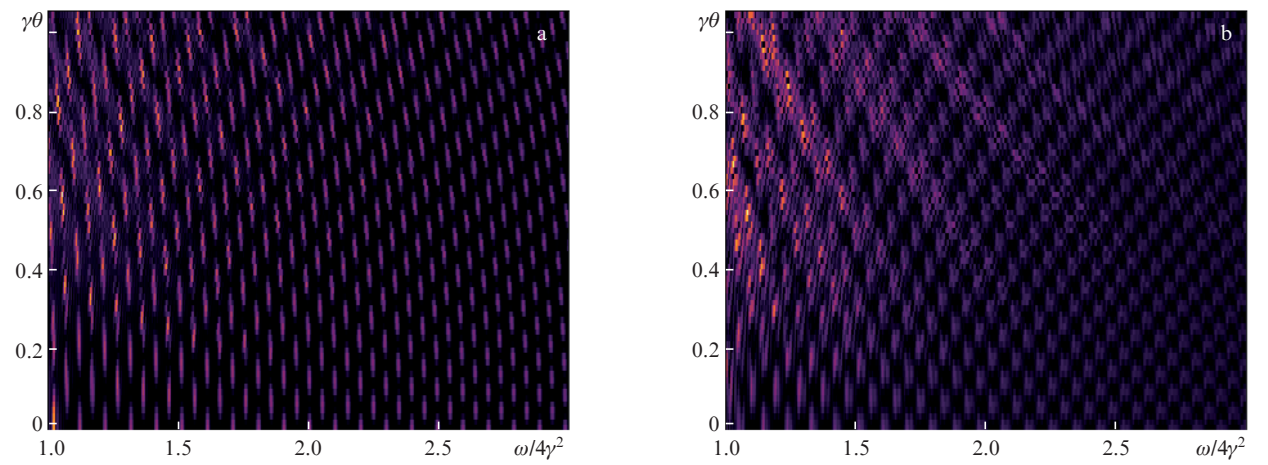

Figure 3. (Colour online) Angular distribution of the spectrum of scattering of an optimally polarisation-gated pulse on a single electron ($\gamma = 1000$) for a polar angle equal to zero at $a_0 = 4$ and $\tau = 16\pi$ (a) without allowance for radiation friction and (b) with allowance for classical radiation friction.

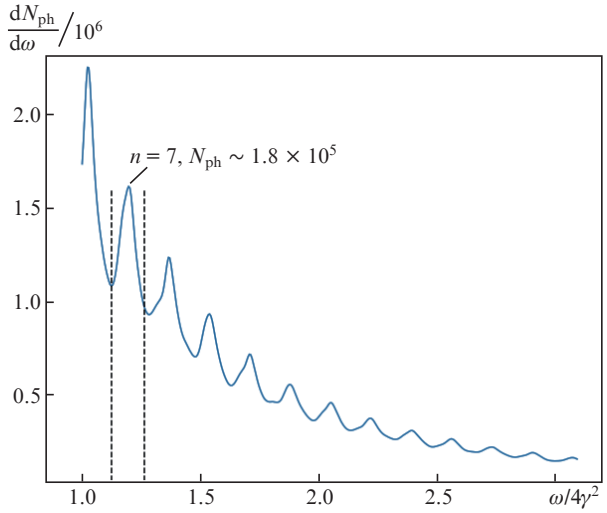

Figure 4. Differential number of photons per unit frequency at $a_0 = 2$, $\tau = 24\pi$, $w_0 = 32$ upon scattering by an electron beam with $\sigma_r = 4.2$, $\sigma_p = 0.3$, $\delta E = 0.1\%$; the collimation angle is $\gamma\theta_{col} = 0.4$.

which should be integrated over the polar angle and the selected collimation angle θ_{col}. Figure 4 shows the differential number of photons per unit frequency for an optimally polarisation-gated pulse ($a_0 = 2$, $\tau = 24\pi$, $w_0 = 32$) on the electron beam ($\sigma_r = 4.2$, $\sigma_p = 0.3$, $\delta E = 0.1\%$). Such radial and angular divergences correspond to the normalised emittance $\epsilon_n \sim 1$ mm mrad. In this case, we used a relatively small collimation angle, $\gamma\theta_{col} = 0.4$. It can be seen that due to a nonideal electron beam, the gamma comb is significantly blurred (which is more noticeable for higher harmonics), but it can still be clearly visible. For the parameters under consideration, the spectral window $\Delta\omega/\omega \approx 0.12$ of the seventh harmonic contains about 10^5 photons, which is comparable to standard photon sources in photonuclear experiments [34].

When considering the electron beam effect on the gamma comb observability, it is necessary to separate two effects: broadening due to ponderomotive scattering of electrons from the focal volume of laser radiation and broadening due to the electron beam imperfection (angular divergence and energy spread). In this regard, Fig. 5 shows the scattering spectrum of laser radiation ($a_0 = 2$, $\tau = 24\pi$, and $w_0 = 32$) on electron beams with different radial divergence ($\sigma_r = 2, 4, 8$) and zero angular divergence and zero energy spread. The upper row corresponds to the backscattered spectrum, while the lower row shows the corresponding angular distributions. It can be seen that already at $\sigma_r = 8$ the broadening becomes noticeable over the entire distance between the harmonics, and after collimation, the picture becomes even more blurred. Separately, it should be noted that in the presence of angular divergence or energy spread, the broadening from ponderomotive scattering is even higher.

A large radial divergence is expressed in a more noticeable ponderomotive scattering, and the effects of angular divergence and energy spread are the same: an electron with an energy other than the central one and not in the beam focus will emit other frequencies [different from the central ones from Eqn (7)], and so the final spectrum will consist of a wider frequency range, resulting in substantial broadening. Figure 6

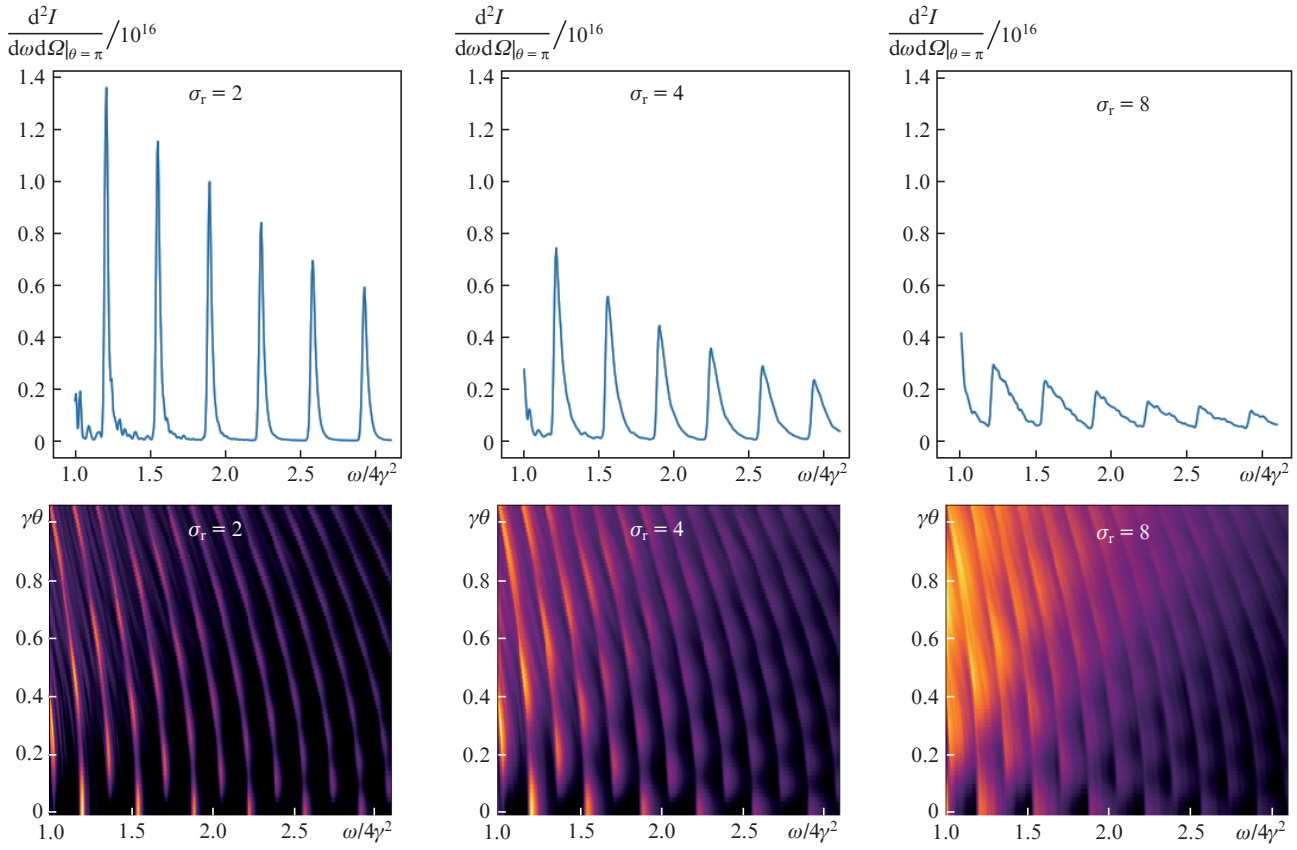

Figure 5. (Colour online) Backscattered spectrum (top row) and angular distribution (bottom row) in the case of scattering of an optimal polarisation-gated pulse by an electron beam at $a_0 = 2$, $\tau = 24\pi$, $w_0 = 32$ and various radial divergence σ_r.

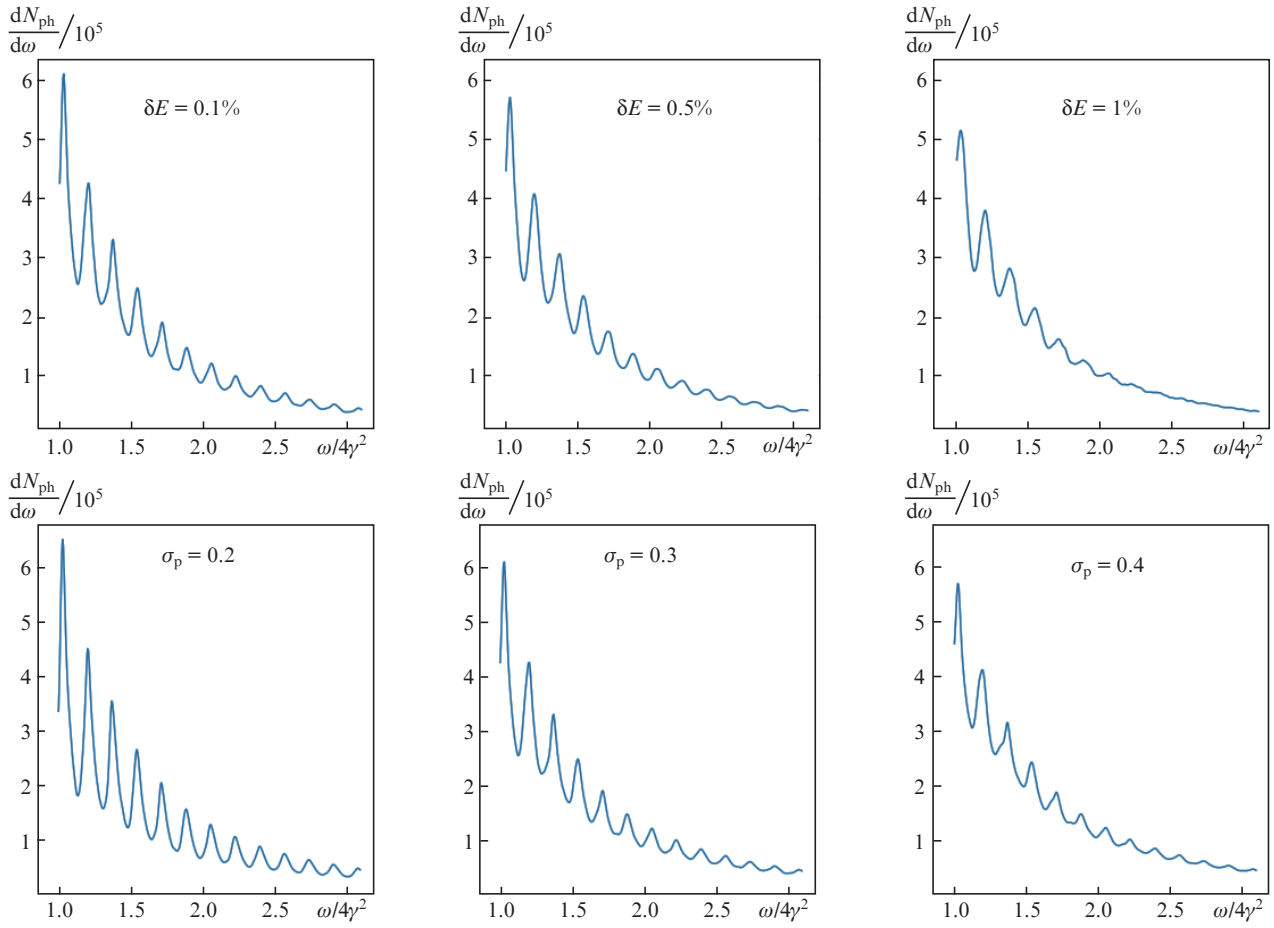

Figure 6. Differential number of photons per unit frequency at $a_0 = 2$, $\tau = 24\pi$, $w_0 = 32$, $\sigma_r = 4.2$ and various values of angular divergence and energy spread for $\sigma_p = 0.3$ for different δE (top row) and σ_p, $\delta E = 0.1\%$ (bottom row). Collimation angle is $\gamma\theta_{col} = 0.2$.

shows the differential number of photons for electron beams with various energy spreads and angular divergences. It can be seen that for a sufficiently large divergence, the gamma comb is still visible, but for less ideal beams the high harmonics are completely blurred (see the case $\delta E = 1\%$).

When considering scattering by a single electron, we have shown that nonlinear effects increase with increasing laser intensity, while the spectral distance between the harmonics decreases, and if it were not for the polarisation gating technique, the spectra of the first and third harmonics would already overlap for $a_0 \geqslant 2$. Figure 7 shows the results for various laser intensities ($a_0 = 1.5$, 2, 2.5). As the laser intensity increases, the gamma comb becomes more and more blurred.

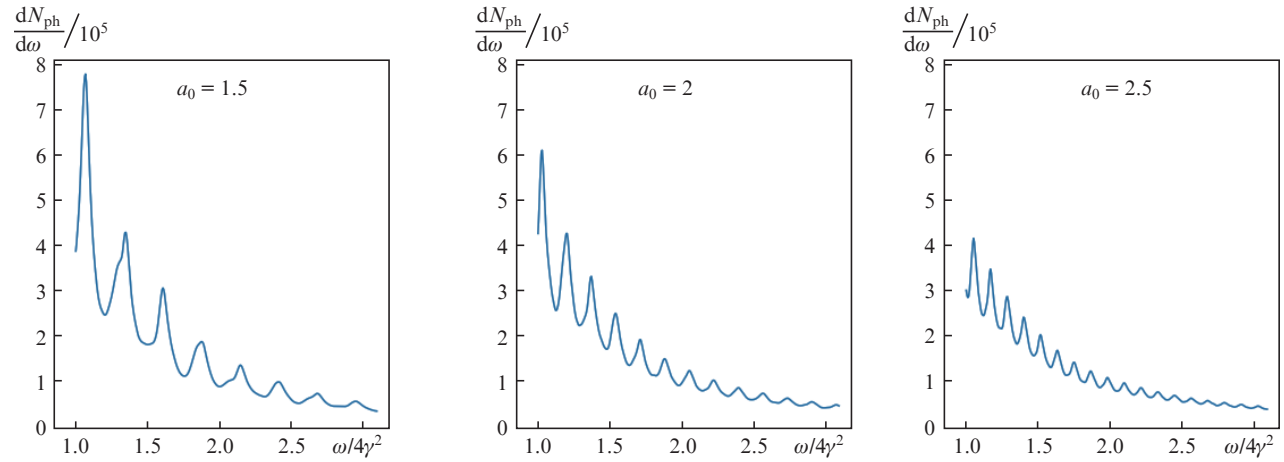

Figure 7. Differential number of photons per unit frequency for $\tau = 24\pi$, $w_0 = 32$, $\sigma_r = 4.2$, $\sigma_p = 0.3$, $\delta E = 0.1\%$ and different a_0. Collimation angle is $\gamma\theta_{col} = 0.2$.

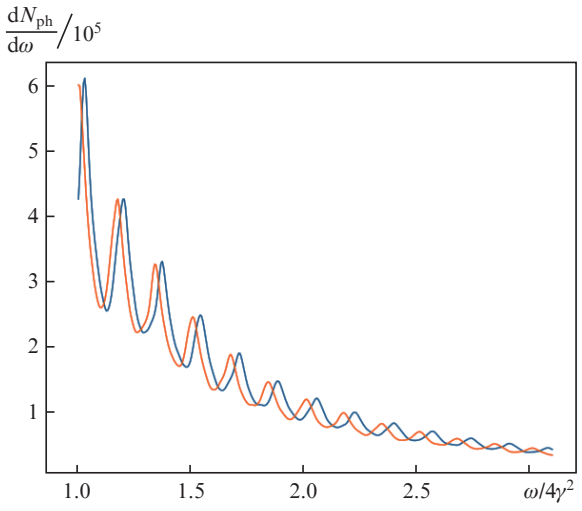

Figure 8. (Colour online) Differential number of photons per unit frequency at $a_0 = 2$, $\tau = 24\pi$, $w_0 = 32$, $\sigma_r = 4.2$, $\sigma_p = 0.3$, $\delta E = 0.1\%$, calculated with allowance (orange curve) and without allowance (blue curve) for radiation friction. Collimation angle is $\gamma\theta_{col} = 0.2$.

Considering the effect of radiation friction and electron recoil, we mentioned that for the parameters used, the broadening caused by these effects will not be very significant against the background of the broadening due to the electron beam nonideality. It can be seen from Fig. 8 that the contribution of radiation friction is only reduced to the red shift, which can probably be measured experimentally.

4. Conclusions

Recently, it has been proposed to use laser pulses with time-dependent ellipticity (polarisation gating technique) to significantly reduce the ponderomotive broadening of the harmonics of Compton scattering. This method leads to the formation of a narrow gamma comb in the spectrum. We have considered the effect of classical radiation friction and electron recoil on the gamma comb in the case of scattering by a single electron. The proposed method can be used for experimental measurement of the quantum shift – the difference between the harmonic position and its classical prediction. A fairly detailed numerical study of the effect of the electron beam nonideality on the gamma comb observability is also given. For laser beams with a focal spot size several times larger than the electron beam size, it has been demonstrated that the gamma comb spectrum is preserved for a wide range of electron beam parameters. The polarisation gating technique is pretty easy to implement experimentally and, apparently, the gamma comb can be observed experimentally for quite standard electron beams.

Acknowledgements. The numerical results presented in this work were obtained using the Zhores cluster of the Skolkovo Institute of Science and Technology [35].

References

1. Faure J., Glinec Y., Pukhov A., Kiselev S., Gordienko S., Lefebvre E., Rousseau J.P., Burgy F., Malka V. *Nature*, **431**, 541 (2004).
2. Mangles S.P., Murphy C.D., Najmudin Z., Thomas A.G., Collier J.L., Dangor A.E., Divall E.J., Foster P.S., Gallacher J.G., Hooker C.J., Jaroszynski D.A. *Nature*, **431**, 535 (2004).
3. Geddes C.G., Toth C., Van Tilborg J., Esarey E., Schroeder C.B., Bruhwiler D., Nieter C., Cary J., Leemans W.P. *Nature*, **431**, 538 (2004).
4. Nedorezov V.G., Turinge A.A., Shatunov Yu.M. *Phys. Usp.*, **47**, 341 (2004) [*Usp. Fiz. Nauk*, **174**, 353 (2004)].
5. Nedorezov V.G., Rykovanov S.G., Savel'ev A.B. doi: 10.3367/UFNr.2021.03.038960.
6. Geddes C.G., Rykovanov S., Matlis N.H., Steinke S., Vay J.-L., Esarey E.H., Ludewigt B., Nakamura K., Quiter B.J., Schroeder C.B., et al. *Nucl. Instrum. Methods Phys. Res. B*, **350**, 116 (2015).
7. Carroll F.E., Mendenhall M.H., Traeger R.H., Brau C., Waters J.W. *Am. J. Roentgenol.*, **181** (5), 1197 (2003).
8. Weeks K., Litvinenko V., Madey J. *Medical Phys.*, **24**, 417 (1997).
9. Tommasini R., Hatchett S.P., Hey D.S., Iglesias C., Izumi N., Koch J.A., Landen O.L., MacKinnon A.J., Sorce C., Delettrez J.A., Glebov V.Y., Sangster T.C., Stoeckl C. *Phys. Plasmas*, **18**, 056309 (2011).
10. Toyokawa H., Ohgaki H., Mikado T., Yamada K. *Rev. Sci. Instrum.*, **73**, 3358 (2002).
11. Quiter B.J., Prussin S.G., Pohl B., Hall J., Trebes J., Stone G., Descalle M.A. *J. Appl. Phys.*, **103** (6), 064910 (2008).
12. Hartemann F.V., Troha A.L., Luhmann Jr N.C., Toffano Z. *Phys. Rev. E*, **54** (3), 2956 (1996).
13. Hartemann F.V., Wu S.S. *Phys. Rev. Lett.*, **111**, 044801 (2013).
14. Rykovanov S., Geddes C., Schroeder C., Esarey E., Leemans W. *Phys. Rev. Accel. Beams*, **19**, 030701 (2016).
15. Heinzl T., Seipt D., Kämpfer B. *Phys. Rev. A*, **81**, 022125 (2010).
16. Seipt D., Kämpfer B. *Phys. Rev. A*, **83**, 022101 (2011).
17. Ghebregziabher I., Shadwick B.A., Umstadter D. *Phys. Rev. Spec. Topics-Accel. Beams*, **16**, 030705 (2013).
18. Terzíc B., Deitrick K., Hofler A.S., Krafft G.A. *Phys. Rev. Lett.*, **112**, 074801 (2014).
19. Seipt D., Rykovanov S., Surzhykov A., Fritzsche S. *Phys. Rev. A*, **91**, 033402 (2015).
20. Kharin V.Y., Seipt D., Rykovanov S.G. *Phys. Rev. Lett.*, **120**, 044802 (2018).
21. Seipt D., Kóharin V.Y., Rykovanov S.G. *Phys. Rev. Lett.*, **122**, 204802 (2019).
22. Rykovanov S.G., Geissler M., Meyerter Vehn J., Tsakiris G.D. *New J. Phys.*, **10**, 025025 (2008).
23. Valialshchikov M., Kharin V.Y., Rykovanov S. *Phys. Rev. Lett.*, **126**, 194801 (2021).
24. Esarey E., Ride S.K., Sprangle P. *Phys. Rev. E*, **48**, 3003 (1993).
25. Landau L.D., Lifshits E.M. *Course of Theoretical Physics. Vol. 2. The Classical Theory of Fields* (Oxford, New York, Toronto, Sydney, Braunschweig: Pergamon Press, 1971; Moscow: Nauka, 1967).
26. Thomas A., Ridgers C., Bulanov S., Griffin B., Mangles S. *Phys. Rev. X*, **2**, 041004 (2012).
27. Ruijter M., Kharin V.Y., Rykovanov S. *J. Phys. B*, **51**, 225701 (2018).
28. Di Piazza A. *Lett. Math. Phys.*, **83**, 305 (2008).
29. Jackson J.D. *Classical Electrodynamics* (New York: John Wiley & Sons, 1962; Moscow: Mir, 1965).
30. Kharin V.Y., Seipt D., Rykovanov S. *Phys. Rev. A*, **93**, 063801 (2016).
31. Kharin V.Y., Seipt D., Rykovanov S.G. *Phys. Rev. Lett.*, **120**, 044802 (2018).
32. Chen M., Esarey E., Geddes C., Schroeder C., Plateau G., Bulanov S., Rykovanov S., Leemans W. *Phys. Rev. Spec. Topics-Accel. Beams*, **16**, 030701 (2013).
33. Faatz B., Braune M., Hensler O., Honkavaara K., Kammering R., Kuhlmann M., Ploenjes E., Roensch-Schulenburg J., Schneidmiller E., Schreiber S., et al. *Appl. Sci.*, **7**, 1114 (2017).
34. Weller H.R., Ahmed M.W., Gao H., Tornow W., Wu Y.K., Gai M., Miskimen R. *Progr. Part. Nucl. Phys.*, **62**, 257 (2009).
35. Zacharov I., Arslanov R., Gunin M., Stefonishin D., Bykov A., Pavlov S., Panarin O., Maliutin A., Rykovanov S., Fedorov M. *Open Eng.*, **9**, 512 (2019).